

Localization transition in the presence of cavity backactionKatharina Rojan,^{1,2,3} Rebecca Kraus,¹ Thomás Fogarty,^{1,4} Hessam Habibian,^{1,*} Anna Minguzzi,^{2,3} and Giovanna Morigi¹¹*Theoretische Physik, Universität des Saarlandes, D-66123 Saarbrücken, Germany*²*Université Grenoble-Alpes, LPMMC, Boîte Postale 166, F-38042 Grenoble, France*³*CNRS, LPMMC, Boîte Postale 166, F-38042 Grenoble, France*⁴*Quantum Systems Unit, Okinawa Institute of Science and Technology Graduate University, Okinawa 904-0495, Japan*

(Received 4 May 2016; published 20 July 2016)

We study the localization transition of an atom confined by an external optical lattice in a high-finesse cavity. The atom-cavity coupling yields an effective secondary lattice potential, whose wavelength is incommensurate with the periodicity of the optical lattice. The cavity lattice can induce localization of the atomic wave function analogously to the Aubry-André localization transition. Starting from the master equation for the cavity and the atom we perform a mapping of the system dynamics to a Hubbard Hamiltonian, which can be reduced to the Harper's Hamiltonian in appropriate limits. We evaluate the phase diagram for the atom's ground state and show that the transition between extended and localized wave function is controlled by the strength of the cavity nonlinearity, which determines the size of the localized region and the behavior of the Lyapunov exponent. The Lyapunov exponent, in particular, exhibits resonancelike behavior in correspondence with the optomechanical resonances. Finally we discuss the experimental feasibility of these predictions.

DOI: [10.1103/PhysRevA.94.013839](https://doi.org/10.1103/PhysRevA.94.013839)**I. INTRODUCTION**

Cavity quantum electrodynamics (CQED) with cold atoms provides a rich framework to study the wave-particle duality of light and matter [1–3]. In this environment, the interaction of a single photon with a single atom has been brought to a level of control that is sensitive to the finite spatial localization of the atom within the cavity mode [4–9]. This property is at the basis of several protocols which exploit the optomechanical coupling between atoms and photons in CQED in order to cool the atomic motion [3,10–13], to perform high precision measurements [14,15], and to create novel sources of quantum light [16–19], for example.

Cavity backaction, moreover, modifies the dynamics to the extent that photons and atoms become strongly correlated: Since the photon field depends on the atomic position within the resonator, the mechanical forces that the atom (or molecule) experiences depend on the center-of-mass wave function within the cavity mode [20,21]. This nonlinearity is at the basis of several collective phenomena, such as the formation of spatial patterns [22–24], synchronization [25,26], and exotic phases of ultracold matter [27–30]. Even at the level of a single particle it can give rise to peculiar behaviors, which shed light on the interplay between nonlinear dynamics and quantum fluctuations.

In this work, we theoretically investigate the regime in which cavity backaction can induce the transition to localization of the atomic center-of-mass wave function. The system we consider is illustrated in Fig. 1(a): A single atom is tightly confined by an external optical lattice within a high-finesse cavity; its dipole strongly couples with a standing-wave mode of the resonator. In the regime in which this coupling is dispersive, the mechanical effects of the cavity field are described by a second periodic potential. We choose the two

lattice wavelengths with periods which are incommensurate with each other. The combination of these two characteristic lengths gives rise to an aperiodic, pseudorandom potential.

In the limit where the cavity nonlinearity can be neglected, the system is described by the Aubry-André model [31] or the Harper model [32], which predicts a transition from an extended to a localized phase when the ratio between the depths of the two potentials exceeds a critical value. This localization transition has been observed experimentally with ultracold atoms confined by bichromatic optical lattices by tuning the amplitude of the secondary lattice potential [33–35]. The effect of interactions on the Aubry-André model has been investigated theoretically both in the mean-field weakly interacting regime [36] and for arbitrary interactions at low lattice filling [37,38]. Quasiperiodic potentials have also been realized with exciton polaritons in semiconductor microcavities [39].

Differing from these realizations, the strong coupling with the cavity introduces a novel feature: The depth of the cavity potential, in fact, is proportional to the number of intracavity photons, which is a dynamical variable coupling optomechanically with the atomic motion. In this setting we analyze the localization transition and discuss possible experimental regimes where it could be observed.

This article is organized as follows. In Sec. II we introduce the theoretical model, which encompasses the effect of the cavity nonlinearity, and show how it results from the optomechanical coupling of a single atom with the single mode of a lossy cavity. In Sec. III we analyze the phase diagram for the ground state as a function of the cavity parameters and then discuss experimental realizations in CQED setups. In Sec. IV we draw the conclusions and present outlooks to this work.

II. AUBRY-ANDRÉ'S MODEL IN THE PRESENCE OF CAVITY BACKACTION

In this section we discuss the theoretical model at the basis of our analysis, which is a Hubbard model with the on-site

*Currently at Accenture S.L.U., 08174 Sant Cugat del Vallés, Barcelona, Spain.

energy resulting from a second, incommensurate potential. We then identify the parameters for which one recovers the Aubry-André model [31] or the Harper model [32]. We further discuss the conditions under which the Hubbard model describes a cold atom which optomechanically interacts with the mode of a high-finesse optical cavity.

A. Hubbard model for cavity QED with cold atoms

The model at the basis of our analysis results from the one-dimensional dynamics of a particle of mass m in two periodic potentials, of which one, denoted by $\hat{W}_{\text{ext}}(\hat{x})$, tightly traps the particle at its minima, while the second, $\hat{V}_{\text{eff}}(\hat{x})$, is a perturbation to the first potential, $\hat{H}_{\text{eff}} = \hat{p}^2/(2m) + \hat{W}_{\text{ext}}(\hat{x}) + \hat{V}_{\text{eff}}(\hat{x})$, with \hat{p} and \hat{x} being the canonically conjugate momentum and position. The cavity and external potentials are periodic with wave numbers k and k_0 , respectively, where $k = \beta k_0$ and β is an irrational number. Therefore, the Hamiltonian is aperiodic. Specifically $\hat{W}_{\text{ext}}(\hat{x}) = \hat{W}_{\text{ext}}(\hat{x} + \pi/k_0)$, while $\hat{V}_{\text{eff}}(\hat{x}) = \hat{V}_{\text{eff}}(\hat{x} + \pi/k)$. For later convenience we write $\hat{V}_{\text{eff}}(\hat{x}) = v_0 f(\hat{x})$, where v_0 has the dimensions of an energy and $f(\hat{x}) = f(\hat{x} + \pi/k)$ is a dimensionless function. In the limit in which the dynamics can be restricted to the lowest band of the deep lattice $\hat{W}_{\text{ext}}(\hat{x})$ [40], we can describe it by means of the Hubbard Hamiltonian

$$\hat{H}_{\text{BH}} = -t \sum_{n=1}^{L-1} (|n\rangle\langle n+1| + |n+1\rangle\langle n|) + \sum_{n=1}^L \delta\epsilon_n |n\rangle\langle n|, \quad (1)$$

where $|n\rangle$ denotes the state of the particle at site n of the external lattice potential \hat{W}_{ext} , with $n = 1, \dots, L$ and L being the total number of sites. The Hubbard Hamiltonian is composed of the hopping term, scaled by the tunneling coefficient $t = \langle n|\hat{p}^2/(2m) + \hat{W}_{\text{ext}}(\hat{x})|n+1\rangle$ and by the diagonal term in the basis $\{|n\rangle\}$, whose coefficients are the on-site energy $\delta\epsilon_n = \langle n|\hat{H}_{\text{eff}}|n\rangle$ and which are site dependent since the Hamiltonian is aperiodic. After subtracting an arbitrary energy constant, we can rewrite these coefficients as

$$\delta\epsilon_n = \langle n|\hat{V}_{\text{eff}}(\hat{x})|n\rangle = v_0 \int dx w_n(x) f(x) w_n(x), \quad (2)$$

where $w_n(x) = \langle x|n\rangle$ are the Wannier functions, which are real valued [41].

In the Aubry-André model the site-dependent on-site potential $\delta\epsilon_n$ has the form

$$\delta\epsilon_n = v_0 \cos(2\pi\beta n). \quad (3)$$

The self-duality of the model [31] allows one to show that a continuous transition occurs for the ground state when the value of the energy v_0 reaches a critical potential strength, $v_c^{AA} = 2t$ [32,42]. If $v_0 < v_c^{AA}$ the ground-state wave function is spatially extended, while for $v_0 > v_c^{AA}$ the wave function decays exponentially indicating Anderson-like localization [31,42,43].

In this work, we analyze the localization transition when the incommensurate potential is given by the function

$$f(x) = \arctan[-\delta'_c + C \cos^2(\beta k_0 x)]. \quad (4)$$

The functional form $f(x)$ as given in Eq. (4) is reminiscent of the one considered in Ref. [44] and is typically encountered in optomechanical problems in CQED [27,45–47]. The parameters δ'_c and C are real valued and can take both positive and negative values. The parameter δ'_c is responsible for the appearance of nontrivial poles which can depend on the form of the ground-state wave function and on C . The parameter C controls the functional form of the second potential $f(x)$, as illustrated in Fig. 1(b). The expansion of this potential for small $|C|$ yields the Aubry-André potential (3) to first order in $|C|$: For $|C| \ll 1$ the on-site energy essentially reduces to Eq. (3), with the new amplitude $v'_0 = |C|v_0/[2(\delta_c'^2 + 1)]$. In this limit, we have demonstrated [48] that the critical value at which localization occurs is found at $v'_c = 2t/\alpha$, giving

$$v_c^{\text{cav}} = \frac{4t}{\alpha} \frac{\delta_c'^2 + 1}{|C|}, \quad (5)$$

where the correcting factor α reads $\alpha = \sqrt{A^2 + B^2}$, with $A = -\int dx w_0^2(x) \sin(2\beta k_0 x)$ and $B = \int dx w_0^2(x) \cos(2\beta k_0 x)$ [48]. For $|C| \simeq 1$, the higher harmonics $\cos^{2n} kx$ of the Taylor expansion in C of Eq. (4) becomes relevant and change the functional form of $f(x)$, as illustrated in Fig. 1(b). Differing from the Aubry-André model, this is the regime where the model is not self-dual. In Sec. II B we derive the potential (4) from a microscopic model describing an atom in a high-finesse cavity, subjected to an optical lattice, as in

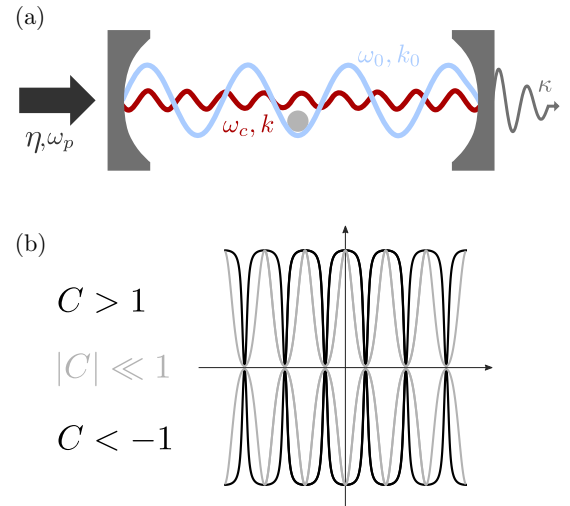


FIG. 1. (a) A single atom is confined by an optical lattice, sketched as blue (light gray) line, with wave number $k_0 = 2\pi/\lambda_0$ and frequency ω_0 within a standing-wave resonator. Its motion optomechanically interacts with a high-finesse mode, shown in red (dark gray), at frequency ω_c and wave number $k = 2\pi/\lambda$, whose wavelength λ is incommensurate with the optical lattice periodicity $\lambda_0/2$. The depth of the cavity lattice is determined by the balance between a pump, with strength η and frequency ω_p , and the losses at rate κ . We study the localization transition in this setup, where the nonlinearity due to strong coupling with the cavity (given by the cooperativity C) modifies the effective incommensurate potential. The optomechanical potential is illustrated in panel (b) as a function of x for three different values of the cooperativity C and when the laser is resonant with the cavity. The limit $|C| \ll 1$ corresponds to the Aubry-André model.

Fig. 1(a). By means of this model one can identify C with the cooperativity of CQED, which measures the strength of the cavity backaction on the atom's scattering properties [49].

In this paper we study the transition to spatial localization. We determine numerically the ground state $|\Psi_0\rangle$ of Hamiltonian (1) with potential (4) as a function of C , δ'_c , and the ratio v_0/t . We characterize the transition by means of the inverse participation ratio P_x [50]:

$$P_x = \sum_{n=1}^L |\langle n|\Psi_0\rangle|^4. \quad (6)$$

The inverse participation ratio (IPR) is of the order $1/L$ if the atom's spatial wave function is uniform over the lattice, whereas it approaches unity when the atom is localized on one single lattice site.

We also monitor the degree of localization by the Lyapunov exponent, defined as [31]

$$\gamma = - \lim_{n \rightarrow \infty} \frac{\ln(|\langle n|\Psi_0\rangle|^2)}{2n}. \quad (7)$$

According to Thouless' formula [51], in the localized regime of the Aubry-André model it reads

$$\gamma = \ln\left(\frac{v_0}{v_c}\right), \quad (8)$$

with $v_c = v_c^{\text{AA}}$ in the case of the original Aubry-André model; i.e., $\delta\epsilon_n$ is given by Eq. (3) and $v_c = v_c^{\text{cav}}$ by Eq. (5). In our calculation we obtain the Lyapunov exponent γ by fitting the spatial decay of the wave function by means of an exponential function.

B. Self-induced localization in CQED

In this section we derive the Hubbard Hamiltonian of Eq. (1) starting from the master equation for the density matrix $\hat{\rho}$ of a linearly polarizable particle and of a lossy cavity field, which strongly couple to one another by means of an optomechanical interaction [52]. In the case of an atom, its dipolar transition is assumed to be driven far-off-resonance by the fields, so that spontaneous decay can be neglected within the typical time scales we consider.

1. Master equation

The relevant degrees of freedom for the atom are the momentum \hat{p} along x and the canonically conjugated position \hat{x} . The cavity mode degrees of freedom are the photon annihilation and creation operators \hat{a} and \hat{a}^\dagger , respectively, with the commutation relation $[\hat{a}, \hat{a}^\dagger] = \hat{1}$. We denote by m the atomic mass and by ω_c the cavity mode frequency, with wavelength $\lambda = 2\pi c/\omega_c$, wave number $k = \beta k_0$, and spatial mode function $\cos(\beta k_0 x)$.

The system is driven by a laser, which is described by a classical field. The laser frequency ω_p is the reference frequency: The atom transition frequency ω_0 is given by the detuning $\Delta_a = \omega_p - \omega_0$ and the cavity mode frequency by the detuning $\delta_c = \omega_p - \omega_c$. In the limit in which $|\Delta_a|$ is the largest frequency characterizing the dynamics, the atom's internal degrees of freedom are eliminated in second-order perturbation theory: In this regime the atomic dipole behaves

as a classical dipole, and its response to the field is described by its polarizability. The dynamics of the density matrix $\hat{\rho}(t)$ describing the state of the atomic center-of-mass position and of the cavity field is governed by the master equation

$$\partial_t \hat{\rho} = \frac{1}{i\hbar} [\hat{H}, \hat{\rho}] + \mathcal{L} \hat{\rho}, \quad (9)$$

where Hamiltonian \hat{H} describes the coherent optomechanical dynamics coupling between the atom's motion and the cavity mode, and the dissipator \mathcal{L} describes cavity losses at rate κ :

$$\mathcal{L} \hat{\rho} = \kappa (2\hat{a} \hat{\rho} \hat{a}^\dagger - \hat{a}^\dagger \hat{a} \hat{\rho} - \hat{\rho} \hat{a}^\dagger \hat{a}). \quad (10)$$

The losses are assumed to be due to the mirror finite transmittivity, while spontaneous decay is neglected assuming that the atomic detuning exceeds the transition linewidth by several orders of magnitude. The Hamiltonian \hat{H} is given by

$$\hat{H} = \frac{\hat{p}^2}{2m} + \hat{W}_{\text{ext}}(\hat{x}) + \hat{H}_{\text{opto}}, \quad (11)$$

where the first term on the right-hand side (RHS) is the kinetic energy and the potential $\hat{W}_{\text{ext}}(\hat{x})$ is periodic with period π/k_0 and tightly binds the atom at its minima,

$$\hat{W}_{\text{ext}}(\hat{x}) = W_0 \cos^2(k_0 \hat{x}),$$

with W_0 being the potential depth with the dimensions of an energy. Hamiltonian \hat{H}_{opto} includes the cavity degrees of freedom and their optomechanical coupling with the atomic motion and reads [20,21]

$$\hat{H}_{\text{opto}} = -\hbar \delta_c \hat{a}^\dagger \hat{a} + \hbar U_0 \cos^2(\beta k_0 \hat{x}) \hat{a}^\dagger \hat{a} + \hbar \zeta(\hat{x})(\hat{a}^\dagger + \hat{a}), \quad (12)$$

where frequency U_0 scales the dynamical Stark shift due to the coupling between the atom and the cavity mode, $U_0 = g^2/\Delta_a$, with the vacuum Rabi frequency g , which determines the strength of the coupling between the dipole and the one-cavity photon. The frequency U_0 can be either positive or negative depending on the sign of Δ_a . The last term on the RHS in Eq. (12) corresponds to the effect induced by an external pump on the cavity mode. The pump, in particular, can couple either directly to the cavity, by impinging on a mirror, or via the atoms, which coherently scatter photons into the cavity mode. When the pump is set directly on the cavity mirror, the strength of this coupling is given by the constant value

$$\zeta(\hat{x}) = \eta. \quad (13)$$

When instead the atom is transversally driven by the laser, then $\zeta(\hat{x})$ takes the form

$$\zeta(\hat{x}) = \cos(\beta k_0 \hat{x}) \Omega g / \Delta_a \quad (14)$$

and is thus weighted by the cavity's spatial mode function at the atomic position. Moreover, it is proportional to the laser Rabi frequency Ω , which determines the strength of the coupling between the dipole and the laser.

2. Time-scale separation and effective dynamics

We consider the limit in which there is a time-scale separation between cavity and atomic motion dynamics and require that the inequality $|\kappa + i\delta_c| \gg k\Delta p/m$ is fulfilled, where $\Delta p = \sqrt{\langle \hat{p}^2 \rangle}$ is the variance of the atomic momentum,

assuming that the cavity linewidth is much larger than the atom Doppler broadening [21]. We then identify the coarse-grained time scale δt , which is sufficiently short with respect to the time scale of the atomic external degrees of freedom and yet sufficiently long that during δt the cavity field reaches a local steady state.

The treatment is best illustrated in the Heisenberg picture and is detailed in Refs. [27,53]. We report here some relevant steps. The equations of motion of the atom and of the cavity field operator read

$$\dot{\hat{p}} = 2\hbar k U_0 \cos(k\hat{x}) \sin(k\hat{x}) \hat{a}^\dagger \hat{a} + 2k_0 W_0 \cos(k_0\hat{x}) \sin(k_0\hat{x}), \quad (15)$$

$$\dot{\hat{a}} = -\kappa \hat{a} + i[\delta_c - U_0 \cos^2(k\hat{x})] \hat{a} - i\eta + \sqrt{2\kappa} \hat{a}_{\text{in}}, \quad (16)$$

if the cavity is pumped by the laser. When the atom is pumped instead, they read

$$\begin{aligned} \dot{\hat{p}} &= 2\hbar k U_0 \cos(k\hat{x}) \sin(k\hat{x}) \hat{a}^\dagger \hat{a} + 2k_0 W_0 \cos(k_0\hat{x}) \sin(k_0\hat{x}) \\ &\quad + \hbar k \frac{\Omega g}{\Delta_a} \sin(k\hat{x}) (\hat{a}^\dagger + \hat{a}), \end{aligned} \quad (17)$$

$$\dot{\hat{a}} = -\kappa \hat{a} + i[\delta_c - U_0 \cos^2(k\hat{x})] \hat{a} - i \frac{\Omega g}{\Delta_a} \cos(k\hat{x}) + \sqrt{2\kappa} \hat{a}_{\text{in}}, \quad (18)$$

where $\hat{a}_{\text{in}}(t)$ is the input noise operator, with $\langle \hat{a}_{\text{in}}(t) \rangle = 0$ and $\langle \hat{a}_{\text{in}}(t) \hat{a}_{\text{in}}^\dagger(t') \rangle = \delta(t - t')$ [54]. Within the time step δt , with $\delta t \gg 1/|\delta_c + i\kappa|$ but yet shorter than the atom's characteristic time scale, we identify the coarse-grained field operator \hat{a}_{st} , which is defined by the equation

$$\int_t^{t+\delta t} \hat{a}(\tau) d\tau / \delta t \approx \hat{a}_{\text{st}},$$

such that $\int_t^{t+\delta t} \dot{\hat{a}}_{\text{st}}(\tau) d\tau = 0$, with $\dot{\hat{a}}$ given in Eq. (16). The “stationary” cavity field is a function of the atomic operators at the same (coarse-grained) time, and in the limit where the quantum noise \hat{a}_{in} averaged over δt can be neglected it takes the form

$$\hat{a}_{\text{st}} \approx \frac{\zeta(\hat{x})}{[\delta_c - U_0 \cos^2(k\hat{x})] + i\kappa}. \quad (19)$$

Notice that this expression corresponds both to the case where the cavity is pumped and to the case where the atom is pumped, by using, respectively, Eq. (13) or Eq. (14) for $\zeta(x)$. A sufficient condition, for which this expression is correct, is that the mean intracavity photon number is larger than unity. A necessary condition, which originates from the statistical averaging at the basis of this treatment, is that $\kappa/\delta t \ll \zeta^2$. In this limit, the field at the cavity output reads

$$\hat{a}_{\text{out}} = \sqrt{2\kappa} \hat{a}_{\text{st}} - \bar{\hat{a}}_{\text{in}} \quad (20)$$

and allows one to monitor the state of the atoms [53–55]. Using Eq. (19) for the field \hat{a} in Eq. (15) leads to an equation of motion for the atomic variables which depends solely on the atomic variables [27]. The corresponding effective Hamiltonian

reads

$$\hat{H}_{\text{eff}} = \frac{\hat{p}^2}{2m} + W_0 \cos^2(k_0\hat{x}) + \hat{V}_{\text{eff}}(\hat{x}), \quad (21)$$

where

$$\hat{V}_{\text{eff}}(\hat{x}) = v_0 f(\hat{x}).$$

Function $f(x)$ is given in Eq. (4), now with $\delta'_c = \delta_c/\kappa$ and $C = U_0/\kappa$, thereby linking the parameters of our model to the microscopic theory. The energy v_0 takes a different form depending on whether the atom or the cavity is driven. When the cavity is pumped, then

$$v_0 = \frac{\hbar}{\kappa} \eta^2, \quad (22)$$

while when the atom is transversally pumped it takes the form

$$v_0 = \hbar \frac{\Omega^2}{\Delta_a} \delta'_c. \quad (23)$$

The Hamiltonian (21) is aperiodic and contains the nonlinear coupling due to the cavity field in the functional form $f(x)$. It can be cast in a Hubbard form using the single-particle Wannier basis $\{w_n\}$ of the external potential. Using this change of basis, in the tight-binding and single-band approximation,

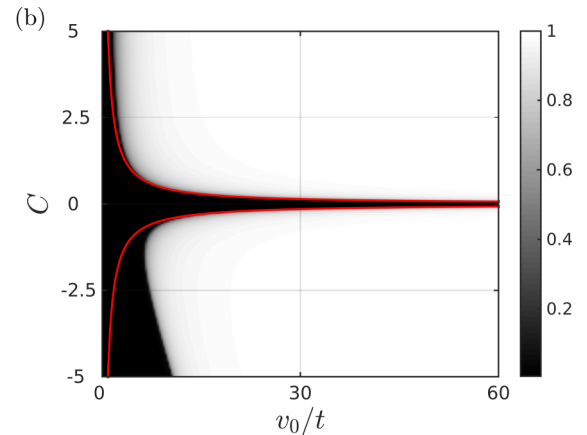
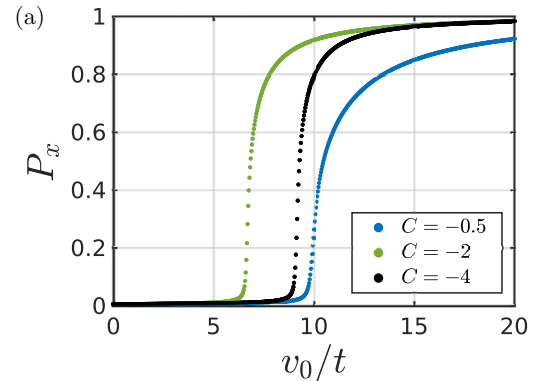


FIG. 2. (a) IPR, Eq. (6), as a function of v_0 (in units of t) for $\delta'_c = 0$ and $C = -0.5, -2$, and -4 (see legend). (b) Contour plot of the IPR as a function of v_0 (in units of t) and of C , for $\delta'_c = 0$. The red (gray) solid lines correspond to Eq. (5). For calculating $\delta\epsilon_n$ in Eq. (4) we used the Wannier function for a confining potential of depth $W_0 = -29E_r$, with $E_r = \hbar^2 k_0^2 / (2m)$ being the recoil energy.

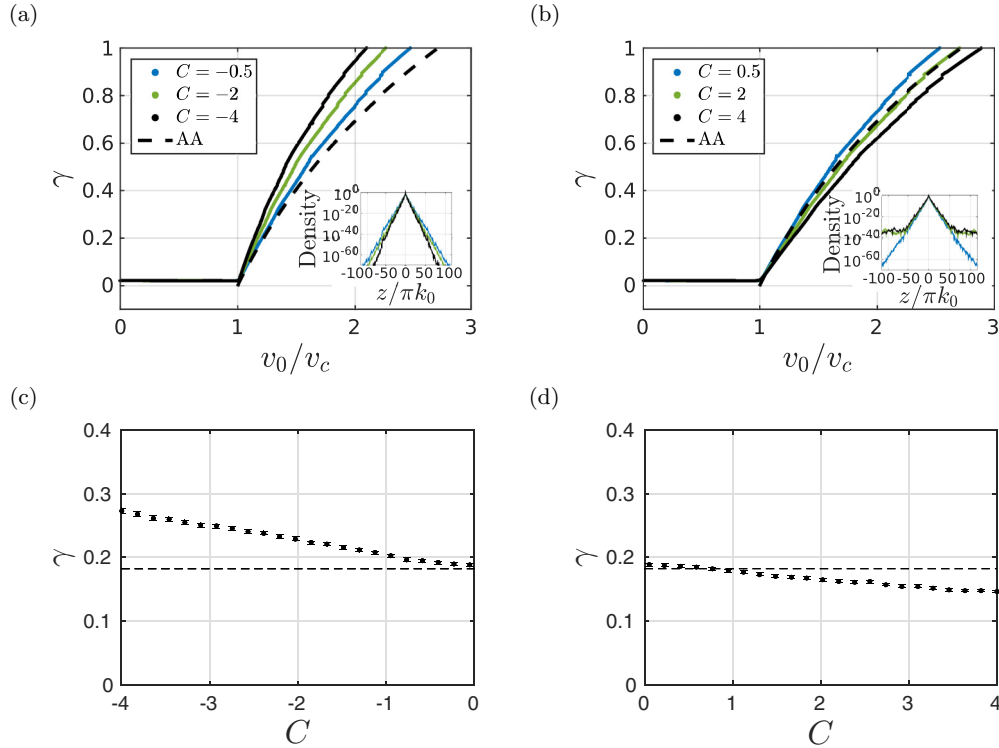


FIG. 3. Lyapunov exponent as a function of v_0 , in units of the critical depth v_c , which we extract from the numerical behavior of the IPR in Fig. 2, for $\delta'_c = 0$ and for (a) $C = -0.5, -2$, and -4 and (b) $C = 0.5, 2$, and 4 . The black dashed line corresponds to the functional behavior of the Lyapunov exponent in Aubry-André's model, Eq. (8). The insets display the probability densities as a function of x for the corresponding values of C of the curves in the onset and for $v_0/v_c = 2$. Panels (c) and (d) display the Lyapunov exponent as a function of C for the fixed ratio $v_0/v_c = 1.2$; the horizontal line indicates the value predicted by Eq. (8) [v_c depends on C , for each value of C it is extracted from the curves of the IPR as in Fig. 2(a)]. For calculating $\delta\epsilon_n$ in Eq. (4) we used the Wannier function for a confining potential of depth $W_0 = -29E_r$, with $E_r = \hbar^2 k_0^2 / (2m)$ being the recoil energy.

one obtains Eq. (1) from Eq. (21), where the on-site energy $\delta\epsilon_n$ is given by Eq. (2), with $f(x)$ as defined in Eq. (4). The tunneling t has the form

$$t = \int dx w_n(x) \left(\frac{-\hbar^2}{2m} \frac{d^2}{dx^2} + W_0 \cos^2(k_0 x) \right) w_{n+1}(x). \quad (24)$$

We have verified that the site-dependent tunneling terms due to the cavity potential,

$$t_n = \int dx w_n(x) V_{\text{eff}}(x) w_{n+1}(x), \quad (25)$$

are negligible for the parameters we choose and that we specify in the next subsection. We remark that, while the resulting dynamics is coherent, its validity relies on a separation between the typical time scales of the cavity, which is intrinsically lossy, and the ones of the atomic motion.

III. RESULTS

In this section we determine the phase diagram for the ground state of Hamiltonian (1), analyze in detail the properties of the localization transition in the framework of CQED, and then discuss possible realizations with existing experimental setups of CQED with cold atoms.

A. Phase diagrams

We determine the IPR, Eq. (6), taking a lattice with open boundaries (hard walls) and choosing $\beta = \frac{\sqrt{5}-1}{2}$. The plots we show are evaluated for $L = 233$. We checked that the IPR and the phase diagrams remain substantially unvaried when scaling up the lattice size L . For this system size, moreover, the behavior of the Lyapunov exponent in the localized phase qualitatively reproduces the thermodynamic limit. We note here that, since the confining lattice has a minimum at $x = 0$, after adding the perturbing potential of Eq. (4) for $C < 0$ the total potential exhibits a minimum at the center, while for $C > 0$ the center is a local maximum [see Fig. 1(b)]. The symmetry by mirror reflection about the center, thus, gives that for $C < 0$ the localized state is in the center, while for $C > 0$ it is a coherent superposition of two sites equally distant from $x = 0$. In order to get a unique localized state for all values of C , for $C > 0$ we take $f(x) = \arctan[-\delta'_c + C \sin^2(\beta k_0 x)]$. This choice allows us to directly compare the localization transition for positive and negative values of C and thus to analyze the sole effect of the potential minimum, which for $C > 0$ is a narrow well and for $C < 0$ is shallow, about $x = 0$.

For all considered values of C and δ'_c the functional behavior of the IPR as a function of v_0 exhibits a sharp transition, as visible in Fig. 2(a) for various values of C . The critical value at which the transition occurs is given in good approximation by the one in Eq. (5) for $|C| \ll 1$, while it differs from this

value the larger $|C|$ becomes. This is clearly visible in Fig. 2(b), which displays the contour plot of the IPR as a function of v_0/t and C for $\delta'_c = 0$. Here, the solid lines correspond to Eq. (5), which predicts the transition value for the corresponding dual model and is visibly shifted with respect to the transition we identify between the extended state (dark region) and the localized state (light region).

We analyze the properties at the transition by plotting the probability density as a function of x and observe that in the localized phase it always exhibits an exponential decay, although for $|C| > 1$ we also find that for the same parameter regimes at large distances the density profile shows an extended component [see insets of Figs. 3(b) and 5]. We have checked that this uniform background is not a numerical artifact. Typical probability densities are shown in the insets of Figs. 3(a) and 3(b). We remark that deviations from a purely exponential profile have been observed in the localized phase of a Bose-Einstein condensate of weakly interacting atoms, where the ground state was the superposition of several localized states [56] due to the effect of interactions. In our case, the observed density profile can be viewed as the overlap between a localized state and an extended state. This behavior is due to the higher harmonics of the cavity potential, Eq. (4): Indeed, we checked that the background appears already by truncating the Taylor expansion of Eq. (4) in $|C|$ to second order (to third order if $\delta'_c = 0$).

Figures 3(a) and 3(b) display the Lyapunov exponent γ as a function of v_0 for $C < 0$ and $C > 0$, respectively. The values are extracted by performing a fit of the central localized region of the density profiles (see insets). This procedure introduces an uncertainty in the determination of the Lyapunov exponent, which is not shown here since it is comparable with the size of the markers. The dependence of γ on C for fixed v_0/v_c is shown in Figs. 3(c) and 3(d), where now the error bars give the uncertainty in the value we fitted. For $C < 0$ the Lyapunov exponent (and thus localization) increases with $|C|$ and is larger than the value of Eq. (8), to which it tends for $C \rightarrow 0^-$. The behavior is qualitatively different for $C > 0$, as visible in Fig. 3(d): As C is increased from 0, the Lyapunov exponent decreases monotonically from the value of Aubry's model. The curve seems to tend to a nonvanishing asymptotic

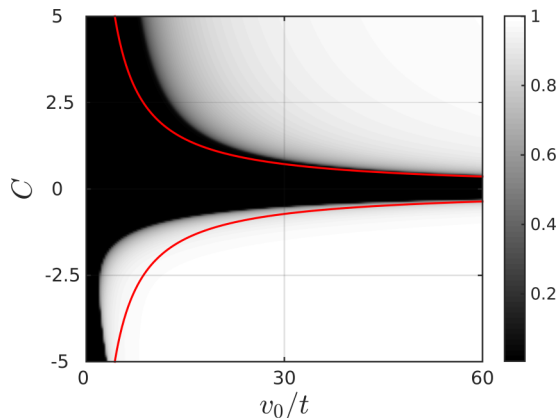


FIG. 4. Contour plot of the IPR as a function of v_0 (in units of t) and of C , for $\delta'_c = -2$. The red (gray) solid lines correspond to Eq. (5). The other parameters are the same as those in Fig. 3.

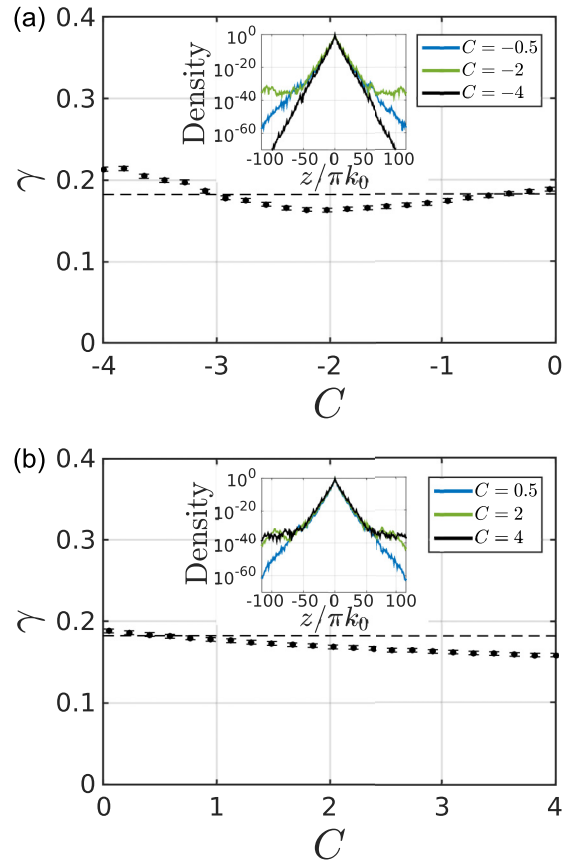


FIG. 5. Panels (a) and (b) display the Lyapunov exponent as a function of C for $v_0/v_c = 1.2$. The black horizontal dashed line indicates the value predicted by Eq. (8). The insets display probability densities as a function of x for different values of C and for the fixed ratio $v_0/v_c = 2$. The other parameters are the same as in those Fig. 3.

constant value for $C \rightarrow \infty$, which is the limit of a sequence of infinitely narrow wells as shown in Fig. 1(b).

We now explore the dependence of γ and of the IPR on the detuning δ'_c . We have checked several values and take $\delta'_c = -2$ in order to provide a representative example. For this value we analyze the IPR (Fig. 4) and the corresponding dependence of the Lyapunov exponents on C (Fig. 5). The contour plot shows that for $C < 0$ the extended phase shrinks with respect to the case $\delta'_c = 0$ [Fig. 2(b)]; the smaller critical value v_c is found at about $C \sim -2$. Correspondingly, the Lyapunov exponent as a function of C possesses a minimum at the same value of the cooperativity. This value is given by a root of the function $f(x)$, Eq. (4), for $\cos^2(kx) \approx 1$, which is fulfilled when the atom is localized at the minimum of the total potential. This root is a resonance which maximizes the intracavity photon number when the atom is in a localized state, as we show below.

B. Experimental realization

Single atoms and ions have been trapped inside cavities and cooled to very low temperatures [1,2]; the dispersive coupling with the cavity field as in Eq. (21) has been realized [3]. These implementations rely on the existence of an external trapping potential, which is typically harmonic. This breaks

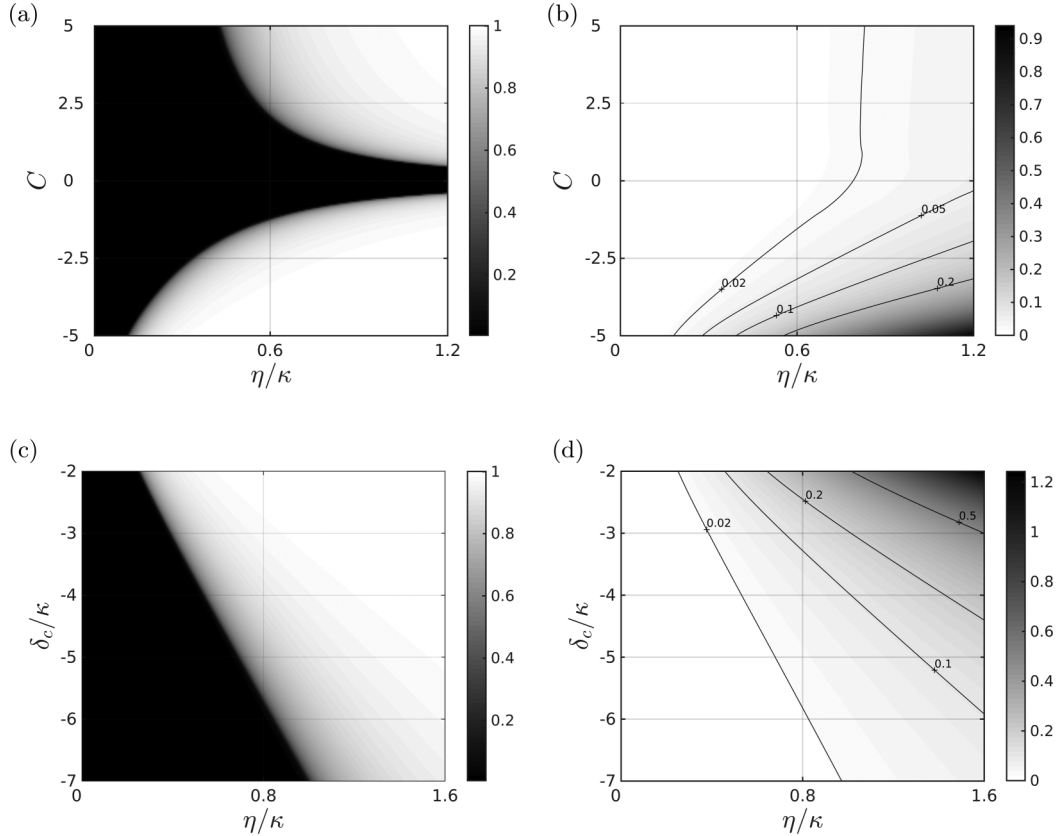


FIG. 6. (a) Inverse participation ratio, Eq. (6), and (b) mean intracavity photon number \bar{n} , Eq. (26), as a function of the parameters η and $C = U_0/\kappa$ in the setup where the resonator is driven and for detuning $\delta_c = -5.5\kappa$. Here, η is the strength of the laser and U_0 is the strength of the optomechanical coupling. In panels (a) and (b) the potential depth is fixed to $W_0 = -15E_r$, where E_r is the recoil energy associated with the D line of ^{87}Rb atoms. Panels (c) and (d) show the IPR and \bar{n} as a function of η and δ_c (in units of κ) for $C = -1$ and $W_0 = -14E_r$. The other parameters are the number of sites $L = 233$ and $\beta = \frac{\sqrt{5}-1}{2}$. For the parameters of Refs. [28,29], where $\kappa \approx E_r/\hbar$, the time-scale separation at the basis of our model is warranted when the detuning $|\delta_c| > E_r/\hbar$ and the atom's temperature $T < 1 \mu\text{K}$.

the discrete translational invariance along the direction of motion thus drastically changing the properties of the extended state. However, a sufficiently shallow trap does not affect the transition to localization as long as the size of the localized state is much smaller than the harmonic oscillator length [33]. Inclusion of the harmonic confinement would be a straightforward extension of the present model. We do not include the harmonic trapping in the present work since under typical experimental conditions (see, e.g., Ref. [28]) the harmonic oscillator length (~ 0.6 for a trapping frequency of $\omega_{\text{ho}} = 2\pi \times 25$ kHz of ^{87}Rb atoms) is much larger than the size of the localized wave function ($\sim 2 \mu\text{m}$ for $\gamma = 0.2$ and $k_0 = 2\pi/830$ nm).

The transition to localization with cold atoms can be revealed by means of time-of-flight measurement, as realized in Ref. [33], or *in situ* imaging [57,58]. Another possibility is to analyze the spectrum of light emitted by the resonator, since this contains the information about the system excitations and allows one to monitor the dynamics [46,55].

The conditions for the time-scale separation we performed in Sec. II B are fulfilled, provided the shot noise component of the cavity field can be neglected over the time scale of the motion, which leads to a condition on the number of intracavity photons and on the atom's kinetic energy. Figures 6(a) and 6(c) display the phase diagram obtained from the IPR, here reported

as a function of the pump strength η , of the cooperativity C , and of the detuning δ_c , for the parameters of the setup of Refs. [28,29]. The transition to localization can be observed for cooperativity $|C| = |U_0|/\kappa \simeq 1$ and thus require the strong coupling at the single-atom level. We further determine the corresponding mean intracavity photon number \bar{n} , according to the equation

$$\begin{aligned} \bar{n} &= \langle \Psi_0 | \hat{a}_{\text{st}}^\dagger \hat{a}_{\text{st}} | \Psi_0 \rangle \\ &\simeq \sum_{m=1}^L | \langle m | \Psi_0 \rangle |^2 \int dz w_m(z)^2 \frac{\zeta^2}{[\delta_c - U_0 \cos^2(k_c z)]^2 + \kappa^2}. \end{aligned} \quad (26)$$

Its form shows that the root of Eq. (4) is an optomechanical resonance in the cavity field [59].

Figures 6(b) and 6(d) show the intracavity photon number for the parameters of the phase diagrams in Figs. 6(a) and 6(c), respectively.

The signal-to-noise ratio can be increased by confining N bosonic atoms in the resonator since the total number of photons scales linearly with the number of atoms N . The dynamics we predict would scale up as long as the atoms form an ideal Bose gas, under similar conditions as the ones realized in the LENS experiment [33,60], such that the

on-site interaction is much smaller than the average kinetic energy at the localization transition. Since the strength of the optomechanical coupling U_0 scales linearly with N [27], sufficiently large atomic samples can allow one to reach the strong-coupling regime, even when for one atom this is not warranted. Nevertheless, for $N > 1$ one shall add to the Hamiltonian governing the dynamics the long-range atom-atom interaction which is mediated by virtual absorption and emission of a cavity photon [27]. We conjecture that in the absence of other types of interactions (such as on-site repulsion) in the ground state, the N atoms will be at the minimum of the single-atom cavity potential, while the excitation spectrum will be relevantly modified.

IV. CONCLUSIONS

We have analyzed the localization transition in a modified Aubry-André model, where the secondary potential, whose periodicity is incommensurate with the confining lattice, is due to the coupling with a high-finesse resonator. Its effective optomechanical potential consists of a transcendental function of the atomic position, which results from the sum of all the harmonics when the light scattered by the atom backacts on the atomic position. In this limit, the localization we predict is self-induced by the atom. We find that it preserves several

features of the Aubry-André model. Novel features are the shift of the localization in the phase diagram and the behavior of the Lyapunov exponent, which is a function of the cooperativity and shows peculiar features close to the parameters where the system exhibits optomechanical resonances.

The localization-delocalization transition we predict can be measured with ideal bosonic gases confined in resonators for existing setups [28,29]. Our study sheds light onto the effect of nonlinearities in the quantum regime and complements the studies on the glassiness of bosons [53] and fermions [61] and on static friction [47] in interacting gases induced by cavity backaction in frustrated geometries.

ACKNOWLEDGMENTS

The authors acknowledge discussions with Stefan Schütz, Simon Jäger, and Astrid Niederle and financial support by the German Research Foundation (DFG Quantum Crystals of Matter and Light), the German Ministry of Education and Research (BMBF “Q.com”), the Laboratoire d’Alliances Nanosciences-Energies du futur (LANEF), and the French-German University (UFA/DFH). A.M. acknowledges financial support from the ANR projects Mathostaq (Grant No. ANR-13-JS01-0005-01) and SuperRing (Grant No. ANR-15-CE30-0012-02).

-
- [1] H. Walther, B. T. H. Varcoe, B.-G. Englert, and T. Becker, *Rep. Prog. Phys.* **69**, 1325 (2006).
 - [2] R. Miller, T. E. Northup, K. M. Birnbaum, A. Boca, A. D. Boozer, and H. J. Kimble, *J. Phys. B: At. Mol. Opt. Phys.* **38**, S551 (2005).
 - [3] H. Ritsch, P. Domokos, F. Brennecke, and T. Esslinger, *Rev. Mod. Phys.* **85**, 553 (2013).
 - [4] C. J. Hood, T. W. Lynn, A. C. Doherty, and H. J. Kimble, *Science* **287**, 1447 (2000).
 - [5] P. W. H. Pinkse, T. Fisher, P. Maunz, and G. Rempe, *Nature (London)* **404**, 365 (2000).
 - [6] G. R. Guthöhrlein, M. Keller, K. Hayasaka, W. Lange, and H. Walther, *Nature (London)* **414**, 49 (2001).
 - [7] B. Casabone, A. Stute, K. Friebe, B. Brandstätter, K. Schüppert, R. Blatt, and T. E. Northup, *Phys. Rev. Lett.* **111**, 100505 (2013).
 - [8] A. Reiserer, N. Kalb, G. Rempe, and S. Ritter, *Nature (London)* **508**, 237 (2014).
 - [9] A. Reiserer and G. Rempe, *Rev. Mod. Phys.* **87**, 1379 (2015).
 - [10] P. Horak, G. Hechenblaikner, K. M. Gheri, and H. Stecher, and H. Ritsch, *Phys. Rev. Lett.* **79**, 4974 (1997).
 - [11] V. Vuletić and S. Chu, *Phys. Rev. Lett.* **84**, 3787 (2000).
 - [12] P. Maunz, T. Puppe, I. Schuster, N. Syassen, P. W. H. Pinkse, and G. Rempe, *Nature (London)* **428**, 50 (2004).
 - [13] T. Kampschulte, W. Alt, S. Manz, M. Martínez-Dorantes, R. Reimann, S. Yoon, D. Meschede, M. Bienert, and G. Morigi, *Phys. Rev. A* **89**, 033404 (2014).
 - [14] S. Schreppler, N. Spethmann, N. Brahms, T. Botter, M. Barrios, and D. M. Stamper-Kurn, *Science* **344**, 1486 (2014).
 - [15] F. Haas, J. Volz, R. Gehr, J. Reichel, and J. Estève, *Science* **344**, 180 (2014).
 - [16] A. S. Parkins and H. J. Kimble, *J. Opt. B* **1**, 496 (1999).
 - [17] G. Morigi, J. Eschner, S. Mancini, and D. Vitali, *Phys. Rev. Lett.* **96**, 023601 (2006).
 - [18] R. Reimann, W. Alt, T. Kampschulte, T. Macha, L. Ratschbacher, N. Thau, S. Yoon, and D. Meschede, *Phys. Rev. Lett.* **114**, 023601 (2015).
 - [19] A. Neuzner, M. Körber, O. Morin, S. Ritter, and G. Rempe, *Nat. Photonics* **10**, 303 (2016).
 - [20] P. Domokos and H. Ritsch, *J. Opt. Soc. Am. B* **20**, 1098 (2003).
 - [21] S. Schütz, H. Habibian, and G. Morigi, *Phys. Rev. A* **88**, 033427 (2013).
 - [22] A. T. Black, H. W. Chan, and V. Vuletić, *Phys. Rev. Lett.* **91**, 203001 (2003).
 - [23] K. Baumann, C. Guerlin, F. Brennecke, and T. Esslinger, *Nature (London)* **464**, 1301 (2010).
 - [24] K. Baumann, R. Mottl, F. Brennecke, and T. Esslinger, *Phys. Rev. Lett.* **107**, 140402 (2011).
 - [25] C. von Cube, S. Slama, D. Kruse, C. Zimmermann, Ph. W. Courteille, G. R. M. Robb, N. Piovela, and R. Bonifacio, *Phys. Rev. Lett.* **93**, 083601 (2004).
 - [26] B. Zhu, J. Schachenmayer, M. Xu, F. Herrera, J. G. Restrepo, M. J. Holland, and A. M. Rey, *New J. Phys.* **17**, 083063 (2015).
 - [27] J. Larson, B. Damski, G. Morigi, and M. Lewenstein, *Phys. Rev. Lett.* **100**, 050401 (2008); J. Larson, S. Fernández-Vidal, G. Morigi, and M. Lewenstein, *New J. Phys.* **10**, 045002 (2008).
 - [28] M. Wolke, J. Klinner, H. Keßler, and A. Hemmerich, *Science* **337**, 75 (2012).
 - [29] J. Klinder, H. Keßler, M. R. Bakhtiari, M. Thorwart, and A. Hemmerich, *Phys. Rev. Lett.* **115**, 230403 (2015).
 - [30] R. Landig, L. Hruby, N. Dogra, M. Landini, R. Mottl, T. Donner, and T. Esslinger, *Nature (London)* **532**, 476 (2016).
 - [31] S. Aubry and G. André, *Ann. Isr. Phys. Soc.* **3**, 133 (1980).

- [32] P. G. Harper, *Proc. Phys. Soc. A* **68**, 874 (1955).
- [33] G. Roati, Ch. D'Errico, L. Fallani, M. Fattori, Ch. Fort, M. Zaccanti, G. Modugno, M. Modugno, and M. Inguscio, *Nature (London)* **453**, 895 (2008).
- [34] M. Schreiber, S. S. Hodgman, P. Bordia, H. P. Lüschen, M. H. Fischer, R. Vosk, E. Altman, U. Schneider, and I. Bloch, *Science* **349**, 842 (2015).
- [35] C. D'Errico, M. Moratti, E. Lucioni, and L. Tanzi, B. Deissler, M. Inguscio, G. Modugno, M. B. Plenio, and F. Caruso, *New J. Phys.* **15**, 045007 (2013).
- [36] G. Modugno, *Rep. Prog. Phys.* **73**, 102401 (2010).
- [37] X. Deng, R. Citro, A. Minguzzi, and E. Orignac, *Phys. Rev. A* **78**, 013625 (2008).
- [38] G. Roux, T. Barthel, I. P. McCulloch, C. Kollath, U. Schollwöck, and T. Giamarchi, *Phys. Rev. A* **78**, 023628 (2008).
- [39] D. Tanese, E. Gurevich, F. Baboux, T. Jacqmin, A. Lemaître, E. Galopin, I. Sagnes, A. Amo, J. Bloch, and E. Akkermans, *Phys. Rev. Lett.* **112**, 146404 (2014).
- [40] V. Guarrera, L. Fallani, J. E. Lye, C. Fort, and M. Inguscio, *New J. Phys.* **9**, 107 (2007).
- [41] W. Kohn, *Phys. Rev.* **115**, 809 (1959).
- [42] Ch. Aulbach, A. Wobst, G. Ingold, P. Hänggi, and I. Varga, *New J. Phys.* **6**, 70 (2004).
- [43] P. W. Anderson, *Phys. Rev.* **109**, 1492 (1958).
- [44] M. Peyrard and M. Remoissenet, *Phys. Rev. B* **26**, 2886 (1982).
- [45] J. K. Asbóth, P. Domokos, and H. Ritsch, *Phys. Rev. A* **70**, 013414 (2004).
- [46] C. Cormick and G. Morigi, *Phys. Rev. A* **87**, 013829 (2013).
- [47] T. Fogarty, C. Cormick, H. Landa, V. M. Stojanović, E. Demler, and G. Morigi, *Phys. Rev. Lett.* **115**, 233602 (2015).
- [48] K. Rojan *et al.* (unpublished).
- [49] H. J. Kimble, in *Cavity Quantum Electrodynamics*, edited by P. R. Berman (Academic, New York, 1994), p. 203.
- [50] D. J. Thouless, *Phys. Rep.* **13**, 93 (1974).
- [51] D. J. Thouless, *Phys. Rev. B* **28**, 4272 (1983).
- [52] A. Vukics and P. Domokos, *Phys. Rev. A* **72**, 031401(R) (2005).
- [53] H. Habibian, A. Winter, S. Paganelli, H. Rieger, and G. Morigi, *Phys. Rev. Lett.* **110**, 075304 (2013).
- [54] C. W. Gardiner and M. J. Collett, *Phys. Rev. A* **31**, 3761 (1985).
- [55] I. B. Mekhov, C. Maschler, and H. Ritsch, *Nat. Phys.* **3**, 319 (2007).
- [56] T. Schulte, S. Drenkelforth, J. Kruse, W. Ertmer, J. Arlt, K. Sacha, J. Zakrzewski, and M. Lewenstein *Phys. Rev. Lett.* **95**, 170411 (2005).
- [57] J. F. Sherson, Ch. Weitenberg, M. Endres, M. Cheneau, I. Bloch, and S. Kuhr, *Nature (London)* **467**, 68 (2010).
- [58] E. Haller, A. K. Hudson, D. A. Cotta, B. Peaudecerf, G. D. Bruce, and S. Kuhrm Stefan, *Nat. Phys.* **11**, 738 (2015).
- [59] S. Gupta, K. L. Moore, K. W. Murch, and D. M. Stamper-Kurn, *Phys. Rev. Lett.* **99**, 213601 (2007); T. P. Purdy, D. W. C. Brooks, T. Botter, N. Brahm, Z.-Y. Ma, and D. M. Stamper-Kurn, *ibid.* **105**, 133602 (2010).
- [60] M. Modugno, *New J. Phys.* **11**, 033023 (2009).
- [61] M. Müller, P. Strack, and S. Sachdev, *Phys. Rev. A* **86**, 023604 (2012).